European Review for Medical and Pharmacological Sciences 2022; 26: 8969-8983

Acceleration of bone repair in critical-size defect using angiopoietin-2 associated with novel carbon nanotubes scaffold *via* mitophagy-pyroptosis pathway

J. YIN[1,2], Z.-Y. TAI[1], Q. HU[1], Y. LIU[1], B. WANG[1], C. ZHU[1], X.-H. LIU[1]

[1]Department of Orthopedics, The Affiliated Jiangning Hospital with Nanjing Medical University, Nanjing, Jiangsu, China
[2]Department of Orthopedics, Shanghai General Hospital of Nanjing Medical University, Songjiang, Shanghai, China

Jian Yin, Ziyi Tai and Qin Hu contributed equally to this work

Abstract. – OBJECTIVE: To investigate the curative effect of Ang-2 combined with novel carbon nanotubes (CNTs) scaffold critical-size bone defect in rabbits.

MATERIALS AND METHODS: CNTs with good properties were first prepared by freeze-drying method. The mechanical properties and surface hydrophilicity of scaffolds were improved by adjusting the addition ratio of polylactic acid (LPA) and chitin fibers (CHI). After purification and functionalization of CNTs, CNTs/PLA/CHI three-dimensional porous scaffolds were prepared for animal experiments. Subsequently, the CNTs/PLA/CHI scaffolds were implanted into the rabbit critical-sized radius defect model to evaluate the osteogenic properties in vivo. Adult male New Zealand white rabbits were randomly allocated into three groups. Group A was the control group, and both groups B and C underwent radial bone defect surgery and implanted CNTs/PLA/CHI scaffolds. Animals in group C received a daily local injection of 1 mL of 400 ng/mL Ang-2 dissolved in physiological saline in the bone defect area for up to 14 days after surgery, while group B received the same amount of physiological saline.

RESULTS: Scanning electron microscope results showed that the porosity of the CNTs/PLA/CHI three-dimensional porous scaffolds was as high as 80%. The surface contact angle was 35° to 55°, and the hydrophilicity was suitable for cell adhesion and growth. The CNTs/PLA/CHI three-dimensional porous scaffolds had excellent biological properties. The general observation and X-ray imaging after 12 weeks together indicated that the CNTs/PLA/CHI scaffolds could accelerate bone repair with the combination of endogenous angiogenic factor Ang-2. The results of western blotting and histology revealed that the expression of mitophagy proteins LC3, Beclin-1, PINK1 and Parkin was elevated in the new bone, and the expression of pyroptosis proteins Nod-like receptor protein NLRP3, caspase-1 and Gasdermin D (GSDMD) was decreased.

CONCLUSIONS: Ang-2 associated with CNTs/PLA/CHI scaffolds accelerated bone regeneration through autophagy-pyroptosis pathway.

Key Words:
Angiopoietin 2, Carbon nanotubes, Critical-size bone defect, Autophagy, Pyroptosis.

Introduction

Nowadays, the critical-size bone defect (CSD), stemming from trauma, infection, cancer, surgical debridement, or congenital deformities, has become a pervasive and challenging issue in orthopedic surgeries[1,2]. Currently, autografts and allografts are considered as treatment options for bone defect and have achieved good clinical outcomes. However, these treatment methods have limited application due to various disadvantages, including limited availability, immune rejection, severe pain, donor limitations and lesions, surgical complications, and infection[3], which calls for better alternatives. To offset these limitations, development and applications of tissue engineering (TE) have been performing a pivotal role in bone regeneration[4]. Owing to the osteoinductivity and osteoconductivity, bone TE has become an efficient approach for bone repair[5]. Compared with autografts and allografts, the biggest advantage of bone TE is that the source of transplantation

Corresponding Author: Xinhui Liu, MD; e-mail: liuxinhuijnyy@163.com

has no biological restrictions and does not damage the donor. Many kinds of artificial scaffolds have been developed and successfully applied to animal experiments. However, ideal bone TE needs to possess a similar structure with natural bone, preeminent mechanical properties and outstanding of osseous integration performances[6]. Accordingly, carbon nanotubes (CNTs) become potential biological scaffolds due to their excellent biocompatibility and osteogenesis[7,8].

Carbon nanotubes (CNTs) are composed of two-dimensional hexagonal graphite sheets and have been largely investigated for bone TE due to the attractive mechanical, electrical, and chemical properties[9]. Proper scaffold clearance is critical for bone repair. Larger pores above 200 μm are helpful for the ingrowth of cells, blood vessels and tissues. While micropores below 10 μm are used to increase the surface area of the material and enhance the protein adsorption capacity to promote bone tissue formation. Polylactic acid (PLA) and chitin fiber (CHI) have been extensively used as bone TE. Since PLA is degraded into acidity and CHI is degraded into alkalinity, we determined an appropriate ratio of PLA and CHI added in order to make the acidity and alkalinity of the degradation product of the composite material suitable for the human body. Subsequently, we cross-linked PLA and CHI to obtain better scaffold structure and mechanical properties. We used freeze-drying method to prepare CNTs/PLA/CHI three-dimensional porous scaffolds with excellent biological properties in order to make carbon nanotubes more suitable for the treatment of bone defect.

Blood supply is the key to bone defect repair. Cytokines, precursor cells and scaffolds are essential components for bone TE. In recent years, many researches[2,6,8] have focused on the combined use of scaffolds and various cytokines to promote the repair of bone defect. The angiopoietin (Ang) family has important roles in regulating the development and proliferation of blood vessels and lymphatic vessels[10]. In a variety of tumor cells, Ang-2 is closely related to tumor recurrence and metastasis due to its strong pro-angiogenic effect[11,12]. Although increased Ang-2 expression is associated with poor tumor prognosis, we were also inspired by this to combine Ang-2 with traditional hydroxyapatite/collagen scaffolds to repair bone defect and found that Ang-2 promoted angiogenesis and improved repair of bone defect by inducing autophagy. As patterns of regulatory cell death (RCD), autophagy and pyroptosis play important roles in angiogenesis[13-15]. Autophagy is an evolutionarily conserved catabolic process that degrades damaged proteins and organelles through lysosomes. Likewise, pyroptosis is a new pro-inflammatory pattern of RCD, mainly mediated by caspase-1 or caspase-11/4/5. Inflammation is known as one of the fundamental biological factors that affect fracture healing[16]. During the repair of bone defects, we speculate that these two patterns of RCD may conduct mutual crosstalk, which has not been reported so far. Therefore, this study combined Ang-2 and CNTs/PLA/CHI scaffolds with better biomechanical properties to treat radial bone defect in rabbits, and further explored the molecular mechanism of Ang-2 promoting bone angiogenesis in bone TE through scanning electron microscopy (SEM), radiographic examination, histology, and protein expression analysis.

Materials and Methods

Materials

CNTs were purchased from Nanoport co., ltd. (Shenzhen, China). PLA, CHI and pentobarbital were purchased from Sigma Aldrich (Missouri, USA). Ang-2 was purchased from Aladdin Chemistry Co., Ltd. (Shanghai, China). Primary antibodies, including LC3, Beclin-1, PINK1, NLRP3, caspase-1, IL-1β and GSDMD and horseradish peroxidase (HRP)-conjugated secondary antibodies were purchased from Abcam (Cambridge, UK). X-ray equipment was purchased from Siemens (Berlin, Germany). SEM was purchased from Carl Zeiss (Tokyo, Japan). Optical microscope was purchased from Olympus (Tokyo, Japan).

Forty-eight healthy and clean adult New Zealand white rabbits were provided by the Animal Experiment Center of Nanjing Medical University, male or female, with a weight of (3.00 ± 0.30) kg and no skeletal developmental deformities.

CNTs/PLA/CHI Scaffolds Fabrication

First, determine an appropriate ratio of PLA and CHI to be added. Since PLA degrades into acidity and CHI degrades into alkalinity, in order to make the acidity and alkalinity of the degradation product of the composite material suitable for the human body, it is necessary to determine an appropriate ratio of PLA and CHI added. PLA (10,000 Kda) and CHI were soaked in PBS solution containing a certain lysozyme

in different proportions, and the pH value of the soaking solution was measured for a certain period. The addition ratio of PLA and CHI with less pH fluctuation was applied in the next experiments. It was found that when the added mass ratio of PLA and CHI was 4:1, the pH value of the soaking solution was about 7.1, which did not fluctuate little during the entire soaking time and more suitable for the human body (Table I). In order to make the mechanical properties and structure of the material more excellent, PLA and CHI were cross-linked. After many repeated experiments, it was found that the appropriate mass ratio of CHI, PLA and the cross-linking agent N, N'-Dicyclohexylcarbonimide (DCC) was 5:8:4. PLA and DCC were dissolved in dichloromethane, then CHI was added, and the cross-linking was completed overnight after magnetic stirring at 0°C for 3 hours. After that, the CHI was taken out of the solution, washed with dichloromethane and air-dried. To determine the critical length of the cross-linked and non-cross-linked fibers required to strengthen PLA, after repeated experiments, the critical length of CHI was obtained to be 1.0-1.2 mm.

Next, the CNTs were purified and functionalized. Surface modification methods are commonly used to tissue engineer biomaterials for purpose of specific surface properties. The CNTs were heated to 60°C in 6M hydrochloric acid and kept for 3 hours and rinsed with distilled water. After the concentrated hydrochloric acid treatment, the CNTs were treated with a mixed solution of sulfuric acid (98%) and nitric acid (60%). Then the CNTs were placed in the mixed solution. After ultrasonication for 3 hours, the CNTs were repeatedly rinsed with deionized water. The purified carboxylated CNTs were obtained after final drying.

Finally, preparation of CNTs/PLA/CHI three-dimensional porous scaffolds by freeze-drying. PLA with a molecular weight of 1.0×10^5 kDa was dissolved in 1,4-dioxane to prepare a solution with a concentration of 60 g/L. Then added CHI cross-linked with PLA according to the previously determined appropriate addition ratio, stirred magnetically for 4 hours at room temperature, and ultrasonically dispersed for 3 hours. According to the mass ratio of CNTs to PLA, it was divided into low groups (1:3), middle groups (2:3) and high groups (3:3) respectively, and the control group did not add CNTs. Three groups of CNTs/PLA/CHI mixed liquids and a control group of mixed liquids were prepared by magnetic stirring for 3 hours and ultrasonic dispersion for 5 hours at room temperature. The mixed solutions prepared above were quickly poured into polytetrafluoroethylene molds and placed in a -18°C refrigerator for 24 hours. Then the molds were transferred to a freeze dryer for freeze drying for 48 hours, and the organic solvent was vacuumed out. Eventually, the CNTs/PLA/CHI three-dimensional porous scaffolds were obtained.

CNTs/PLA/CHI Three-Dimensional Porous Scaffolds Characterization

The porosity of the material was determined by the liquid displacement method. The size of the scaffold pores was observed by scanning electron microscopy. For SEM detection, samples were fixed in 2% glutaraldehyde phosphate

Table I. Relationship between pH change of material soaking solution and soaking time.

Sample	CHI (%)	pH						
		0 w	2 w	4 w	8 w	12 w	16 w	24 w
PLA	-	6.67	3.27 ± 0.10	3.0 ± 0.08	2.44 ± 0.10	2.40 ± 0.09	2.19 ± 0.07	2.18 ± 0.05
Uncross-linked	5	6.67	6.23 ± 0.05	5.88 ± 0.10	5.45 ± 0.09	5.51 ± 0.11	5.49 ± 0.08	5.62 ± 0.10
	10	6.67	6.37 ± 0.06	5.91 ± 0.08	5.66 ± 0.05	5.92 ± 0.08	5.90 ± 0.10	5.94 ± 0.10
	15	6.67	6.55 ± 0.05	6.02 ± 0.04	5.97 ± 0.09	5.99 ± 0.10	6.15 ± 0.05	6.21 ± 0.07
	20	6.67	6.81 ± 0.04	6.68 ± 0.10	6.97 ± 0.07	7.05 ± 0.09	6.98 ± 0.10	7.02 ± 0.08
	25	6.67	6.93 ± 0.05	7.08 ± 0.10	7.08 ± 0.09	7.11 ± 0.08	7.26 ± 0.10	7.42 ± 0.07
Cross-linked	5	6.67	6.19 ± 0.05	5.85 ± 0.10	5.50 ± 0.09	5.47 ± 0.10	5.52 ± 0.10	5.69 ± 0.10
	10	6.67	6.41 ± 0.07	5.98 ± 0.02	5.69 ± 0.06	5.96 ± 0.05	5.95 ± 0.10	5.99 ± 0.08
	15	6.67	6.60 ± 0.05	6.10 ± 0.07	6.02 ± 0.09	6.06 ± 0.10	6.18 ± 0.04	6.24 ± 0.10
	20	6.67	6.85 ± 0.03	6.71 ± 0.10	7.0 ± 0.06	7.05 ± 0.05	7.0 ± 0.10	7.02 ± 0.08
	25	6.67	6.99 ± 0.08	7.11 ± 0.10	7.10 ± 0.09	7.15 ± 0.10	7.22 ± 0.04	7.45 ± 0.10

solution for 48 hours, washed twice with phosphate-buffered saline and distilled water for 30 minutes each, then dehydrated in a graded alcohol solution and dried in 100% ethanol. The samples were finally sputter-dried with gold before SEM observation. The hydrophilicity of the materials containing different amounts of CNTs was compared by the contact angle experiment. The pH value of the PBS soaking solution of the material was determined. In brief, the scaffolds with CNTs volume content of 5, 10, 15, 20, and 25% were soaked in PBS solution containing a certain amount of lysozyme respectively, and then the containers were sealed and placed in a 37°C incubator without any treatment during the degradation process. According to the soaking time of 2, 4, 8, 12, 16, and 24 weeks, the pH value of the soaking solution in each group of 3 containers was measured with an automatic potentiometric titrator.

Degradation rate of stent materials detected by degrading liquid. Briefly, after the samples were sterilized by cobalt 60 irradiation, they were placed in a PBS degradation solution containing trypsin, and then placed in a sterile box at 37°C. Changed the degradation solution in the bottle weekly. For 4 consecutive weeks, 5 samples of each material were taken every week, filtered with double distilled water and then dried at low temperature. The dry weight of the samples at this time was WT. Calculate the degradation rate according to the formula: degradation rate = (WO – WT) / WP × 100%, where WO was the mass of the sample before degradation, and WP was the sum of the mass of PLA and CHI in the sample. The prepared CNTs/PLA/CHI three-dimensional porous scaffolds were cut into a size of 0.4 cm*0.4 cm*1.5 cm. After being sterilized by cobalt 60 irradiation, the scaffolds were stored at room temperature for future use (Figure 1).

Figure 1. General view of prepared CNTs/PLA/CHI three-dimensional porous scaffolds (0.4 cm* 0.4 cm* 1.5 cm).

Establishment of a Radius Bone Defect Model in the Rabbit

As stated in previous study[17], a total of 48 adult male New Zealand white rabbits (weighing 3.00 ± 0.30) were used in this research. Animal experiments were approved by the Animal Care Committee of Nanjing Medical University (NJMU, Nanjing, China). All animals were anesthetized by intravenous pentobarbital (30 mg/kg). A 15 mm bone defect was created using a micro-oscillating saw in the upper one-third of the radial bones in a randomly selected limb of each rabbit (Figure 2A and B). CNTs/PLA/CHI three-dimensional porous scaffolds prepared before were implanted into the bone defect site. Rabbits were randomly allocated into three groups (n = 16) labeled as control group (group A), CNTs/PLA/CHI group (group B), and CNTs/PLA/CHI + Ang-2 (group C). Animals in group C received a daily local injection of 1 mL of 400 ng/mL Ang-2 dissolved in physiological saline in the bone defect area for up to 14 days after surgery, while group B received the same amount of physiological saline.

General Observations and Radiographic Examination

The diet, mobility, swelling or hematoma edema and local inflammatory reactions of rabbits were observed regularly by visual or manual examination. At 12 weeks after surgery, bone tissues were harvested. Blood vessels on the specimen surface and new callus associated with the fracture stump were observed in the specimens. Sequential radiographs of the surgical limbs were recorded at regular intervals (4, 8 and 12 weeks postoperatively) underwent X-ray (8 ma, 40 mv). Lane-Sandhu scores[18] based on X-ray results were used to assess bone formation by two radiologists in a blinded manner.

Pathological Observation

The specimens at 12 weeks after the operation were placed in 4% paraformaldehyde for 12 hours and fixed in 10% EDTA chelated decalcification solution. After decalcification, gradient alcohol dehydration, and paraffin embedding, serial sections of 5 μm were made along the coronal plane

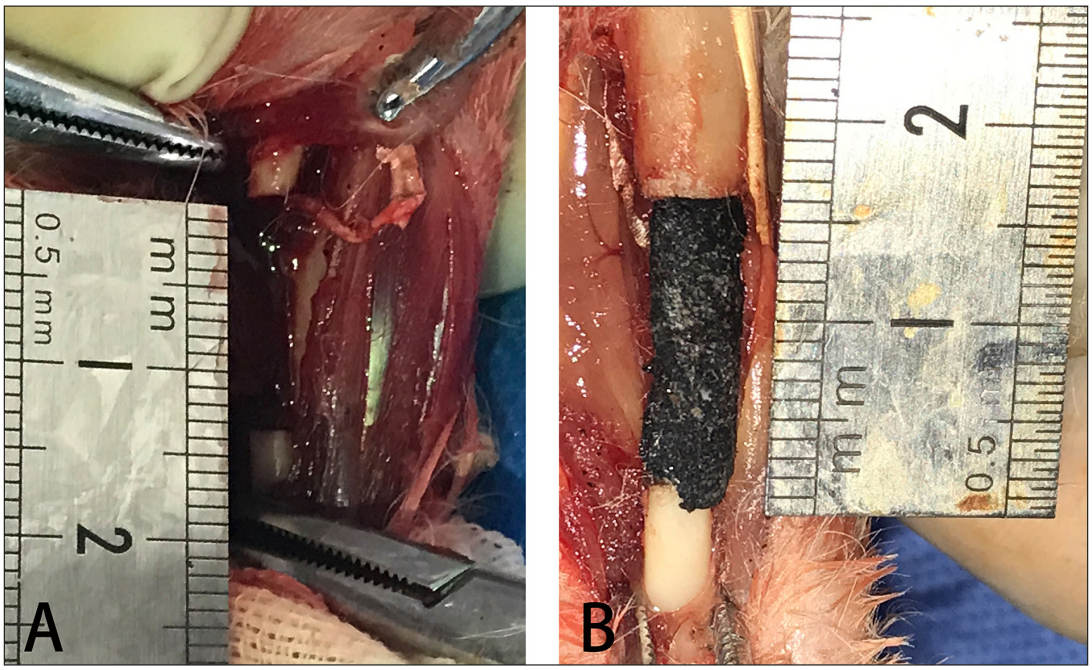

Figure 2. A, Establishment of rabbit radius bone defect model. **B,** CNTs/PLA/CHI scaffold was implanted in the bone defect area, and Ang-2 (1 mL, 400 ng/mL) was injected daily for 14 days after surgery.

of the specimen. After fixation, hydration, hematoxylin staining, differentiation, inverse blue, eosin staining, dehydration, clearing, and mounting, the sections were stained with hematoxylin and eosin (HE). Inverted microscope was used to observe the regeneration of local bone and blood vessels. Six high-power fields (×200) were randomly selected for each slice, and two pathologists with more than five years of working experience counted the number of blood vessels in each slice.

Western Blot Analysis

As described in previous studies[17], in brief, callus tissues in the surgical area were ground by liquid nitrogen, washed and centrifuged. The cell pellet was resuspended in radioimmunoprecipitation assay lysis buffer containing benzene methanesulfonyl fluoride and centrifuged again at 16,000 × g for 15 min at 4°C. The supernatant was saved for protein quantification, and proteins were added to loading buffer for denaturation by heating. The samples were separated on 10% SDS-PAGE and transferred to a polyvinyldifluoride (PVDF) membrane. Subsequently, the membrane was blocked with 5% skimmed milk for 1 h and then incubated with primary antibody overnight and secondary antibody the next day. Reacting bands were visualized using ECL reagents. The protein expression levels in different samples were analyzed using Quantity One software (Bio-Rad, Hercules, CA, USA).

Statistical Analysis

Each experimental indicator was repeated at least three times. Data were presented as means ± standard deviation (SD). Statistical significance was analyzed by the student's *t*-test or one-way analysis of variance (ANOVA) followed by the Tukey-Kramer multiple comparison test using SPSS version 17.0 statistical software (SPSS, Inc., Chicago, IL, USA). *p*-values of less than 0.05 were considered statistically significant.

Results

Characterization of Cnts/PLA/CHI Three-Dimensional Porous Scaffolds

SEM results showed that this three-dimensional porous scaffold possessed a porosity up to 80% (Figure 3 and Table II). It not only contained large pores of more than 200 μm to facilitate the growth of cells, blood vessels and tissues, but also had micropores of less than 10 μm to help increase the surface area of the material and enhance the ability of protein adsorption,

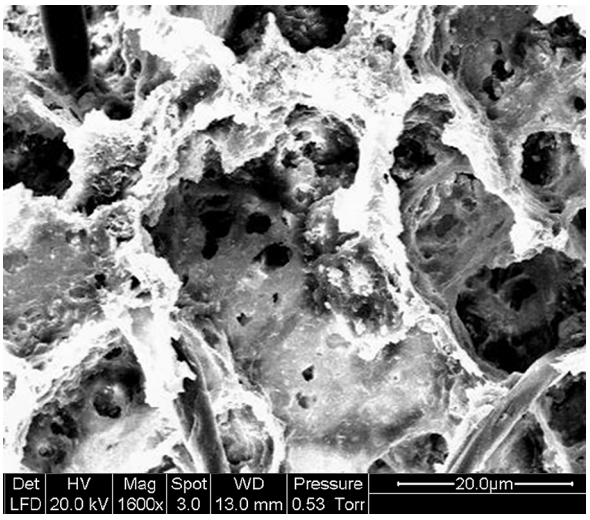

Figure 3. SEM images of CNTs/PLA/CHI scaffolds. The CNTs/PLA/CHI scaffold possessed a porosity up to 80%, and a suitable ratio of macrovoids and microvoids.

which contributed to bone tissue generation. The cross-linking can make the CHI combine with the matrix well, and the contact angle test results of the material showed that the material possessed good hydrophilicity. The surface contact angle of this material was 35° to 55° (Table III), and the hydrophilicity was suitable for cell adhesion and growth (Figure 4).

The pH results demonstrated that the addition of CNTs did not significantly affect the pH of the scaffold material PBS soaking solution. That is to say, it will not significantly affect the acidity and alkalinity of the degradation products of other components. Using the same experimental method, it was found that the pH value of the scaffold material PBS soaking solution was mainly affected by the CHI content. The pH value of PLA soaking solution decreased the fastest with the increase of soaking time, from 6.67 to 2.19 within 16 weeks, and the pH value was almost unchanged from 16 weeks to 24 weeks. With the increase of CHI content, the pH value of stent

Table II. Porosity of CNTs/PLA/CHI scaffolds.

CNTs/PLA ratio	Porosity (%)	
	Uncross-linked	Cross-linked
0:3	90.5 ± 1.5	90.5 ± 1.5
1:3	88.0 ± 1.2	88.0 ± 1.5
2:3	86.5 ± 0.8	86.2 ± 1.0
3:3	83.2 ± 0.8	83.5 ± 0.8

Table III. The surface contact angle of CNTs/PLA/CHI scaffolds.

CNTs/PLA ratio	Angle (°)	
	Uncross-linked	Cross-linked
0:3	35.5 ± 1.9	34.9 ± 2.1
1:3	53.3 ± 2.3	54.5 ± 1.7
2:3	47.6 ± 1.8	48.3 ± 2.6
3:3	43.2 ± 3.0	43.8 ± 1.5

soaking solution decreased gradually with the increase of soaking time (Table I). The *in vitro* degradation rate results indicated that the addition of CNTs did not affect the degradation rates of other components of the material (Table IV). The above results collectively demonstrated that the CNTs/PLA/CHI three-dimensional porous scaffolds possessed excellent biological properties.

General Observation of the Radius

All experimental animals' incisions healed normally, and no experimental animals died. Radius general observation was performed 12 weeks after operation. In group A, only a small amount of callus was formed in the defect area. Both ends of the bone defect were hardened with bone resorption. There was a large amount of inflammatory tissue in the bone defect area. The medullary cavity was closed, and the bone defect was not repaired (Figure 5A and Figure 6A). In group B, a certain amount of callus was formed in the bone defect, however, the defect end was enlarged and hardened. The medullary cavity was closed. A certain amount of inflammatory tissue was distributed in the bone defect area. Although the scaffold was completely degraded,

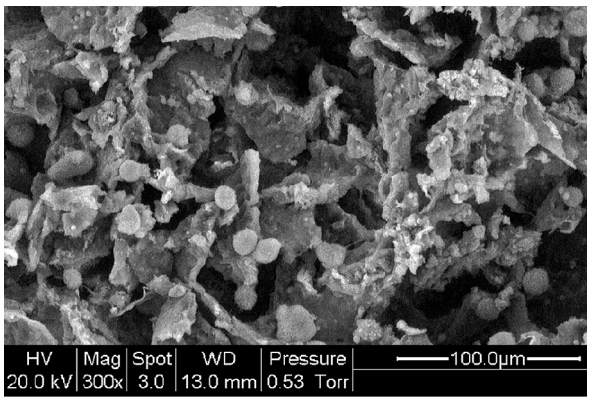

Figure 4. SEM images of CNTs/PLA/CHI scaffolds with excellent adhered of cells and proteins.

Table IV. Degradation rate of scaffold materials *in vitro*.

CNTs/PLA ratio	Degradation rate (%)			
	1 w	2 w	3 w	4 w
0:3	11.25 ± 0.16	16.68 ± 0.31	18.32 ± 0.36	20.23 ± 0.36
1:3	11.21 ± 0.21	16.61 ± 0.26	18.29 ± 0.32	20.16 ± 0.31
2:3	11.19 ± 0.23	16.59 ± 0.22	18.23 ± 0.31	20.12 ± 0.33
3:3	11.26 ± 0.19	16.63 ± 0.35	18.28 ± 0.29	20.19 ± 0.39

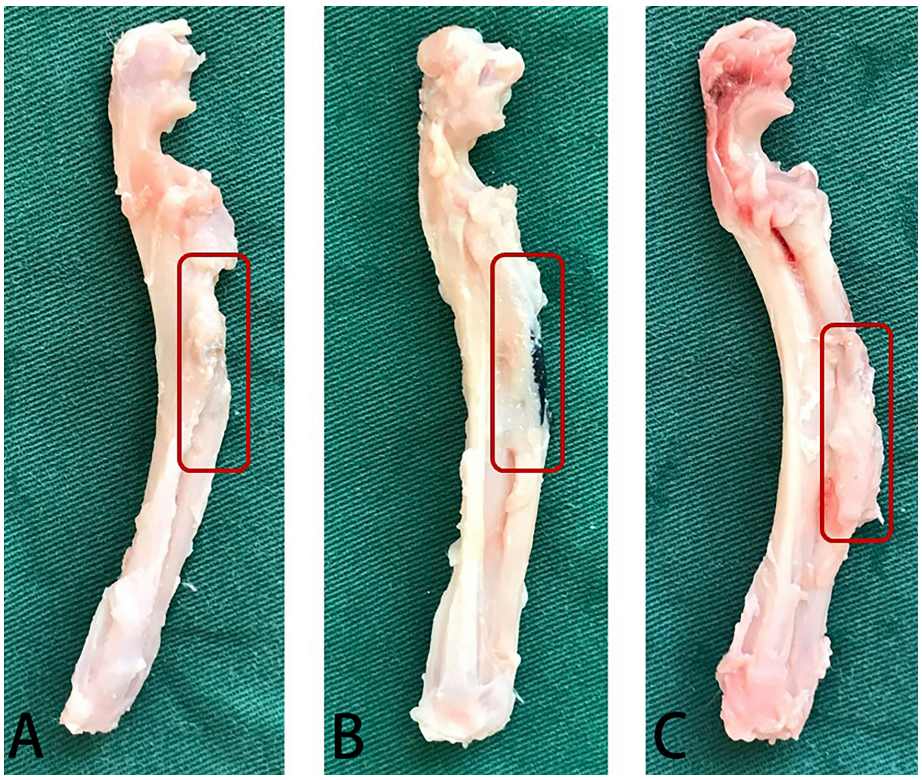

Figure 5. General observation of radial bone defect 12 weeks after surgery. **A**, Group A: Control group; **B**, Group B: CNTs/PLA/CHI group; **C**, Group C: CNTs/PLA/CHI + Ang-2 group.

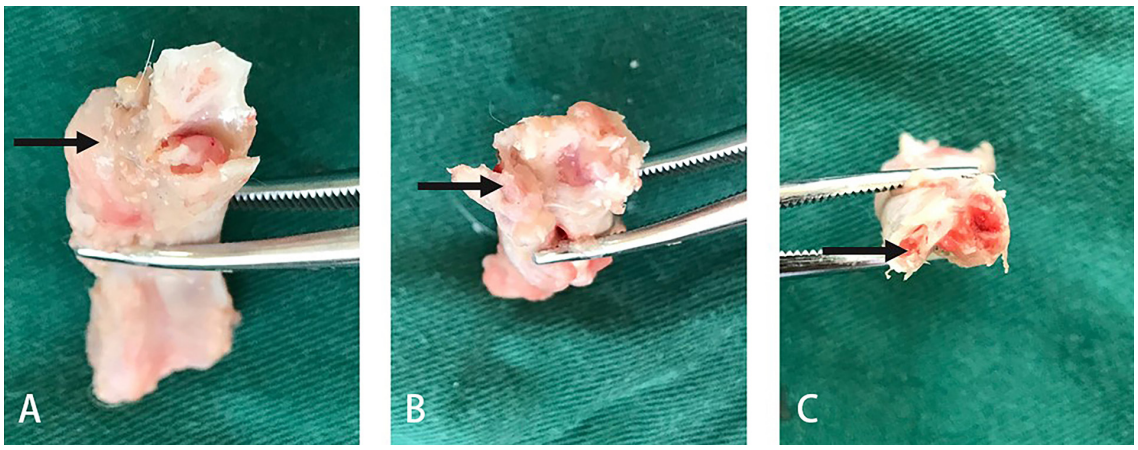

Figure 6. Cross-sectional observation of the bone defect area. **A**, Group A: Control group; **B**, Group B: CNTs/PLA/CHI group; **C**, Group C: CNTs/PLA/CHI + Ang-2 group.

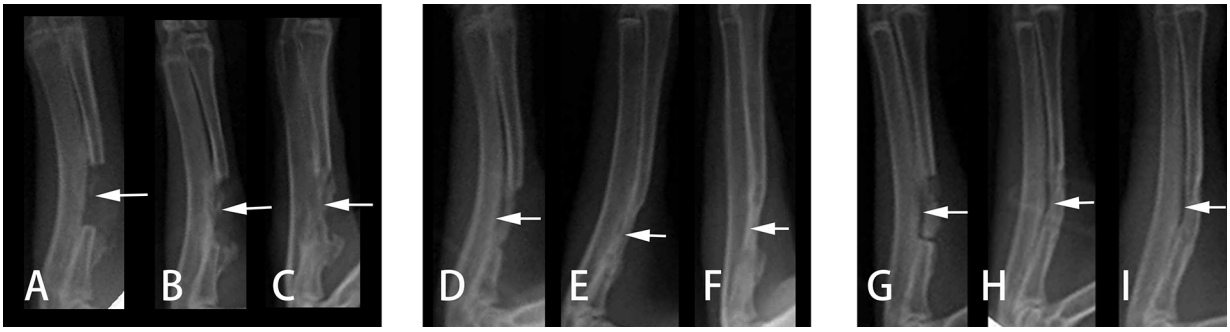

Figure 7. X-ray imaging of rabbit radial bone defect in each group. **A, B,** and **C,** X-ray imaging of rabbit radial bone defect in group A, the control group. **D, E** and **F,** X-ray imaging of group B, with CNTs/PLA/CHI scaffold implanted. **G, H,** and **I,** X-ray imaging of group C, with CNTs/PLA/CHI scaffold implanted and Ang-2 injection. White arrow new callus.

the bone defect was not fully repaired as shown in (Figure 5B and Figure 6B). The growth of callus in group C was obviously accompanied by the restoration of bone continuity. The new bone possessed a tubular shape, and the medullary canal was recanalized. A small amount of inflammatory tissue could be found in the bone defect area. The scaffold was completely degraded (Figure 5C and Figure 6C).

Ang-2 Combined with Cnts/PLA/CHI Scaffolds Promoted the Repair of Bone Defect, as Detected by X-Ray Imaging

Radiographs of the surgical area were performed at 4, 8, and 12 weeks postoperatively. In group A, there was no obvious growth of callus after operation. At 12 weeks after operation, the stump of the bone defect was hardened, and the bone defect area was filled with soft tissue shadows (Figure 7A-C). In group B, less callus growth was observed at 4 weeks postoperatively, and further callus growth was observed at 8 weeks. However, the callus did not increase significantly at 12 weeks after surgery, accompanied by sclerosis of the stump of the bone defect. The nonunion was not completely repaired, but the scaffold was completely degraded (Figure 7D-F). In group C, a certain amount of continuous callus growth was observed 4 weeks after the operation, making both ends of the bone defect continuous. At 8 weeks, the callus further increased, and the new bone thickened. At 12 weeks after operation, the bone marrow cavity was formed. The new bone was further plasticized and the morphology was similar to the surrounding bone tissue. The nonunion was completely repaired and the scaffold was completely degraded (Figure 7G-I).

Ang-2 Combined with Cnts/PLA/CHI Scaffolds Increased Lane-Sandhu Histological Scores

X-ray-based Lane-Sandhu scores were compared in each group (Table V). Scores of group C were significantly higher than those of groups A and B, and the scores of group B were significantly higher compared with group A at each time point. Differences were statistically significant ($p < 0.05$).

Ang-2 Promoted the Formation of New Blood Vessels and the Expression of Vascular Endothelial Growth Factor in the Area of New Callus

At 12 weeks after operation, HE staining exhibited that there were few osteoblasts in group A. The trabecular bone was small and partially broken. The Harvard tube was irregularly arranged and was dominated by braided bone (Figure 8A-B). The number of new blood vessels was low. Group B had a certain number of osteoblasts and lamellar bone, and the trabecular bone was denser (Figure 8C-D). The number of blood vessels was more than that of group A. A large number of osteoblasts was observed in group C. The Harvard tube was neatly arranged, accompa-

Table V. Lane-Sandhu scores of each group at 4, 8 and 12 weeks after surgery.

Group	4 w	8 w	12 w
A (n = 6)	0.17 ± 0.408	2.00 ± 0.894	3.33 ± 1.033
B (n = 6)	1.67 ± 0.816	4.17 ± 0.753	6.33 ± 1.211
C (n = 6)	4.50 ± 0.548	7.67 ± 2.547	9.83 ± 0.753
F	76.912	60.479	61.452
p	0.000	0.000	0.000

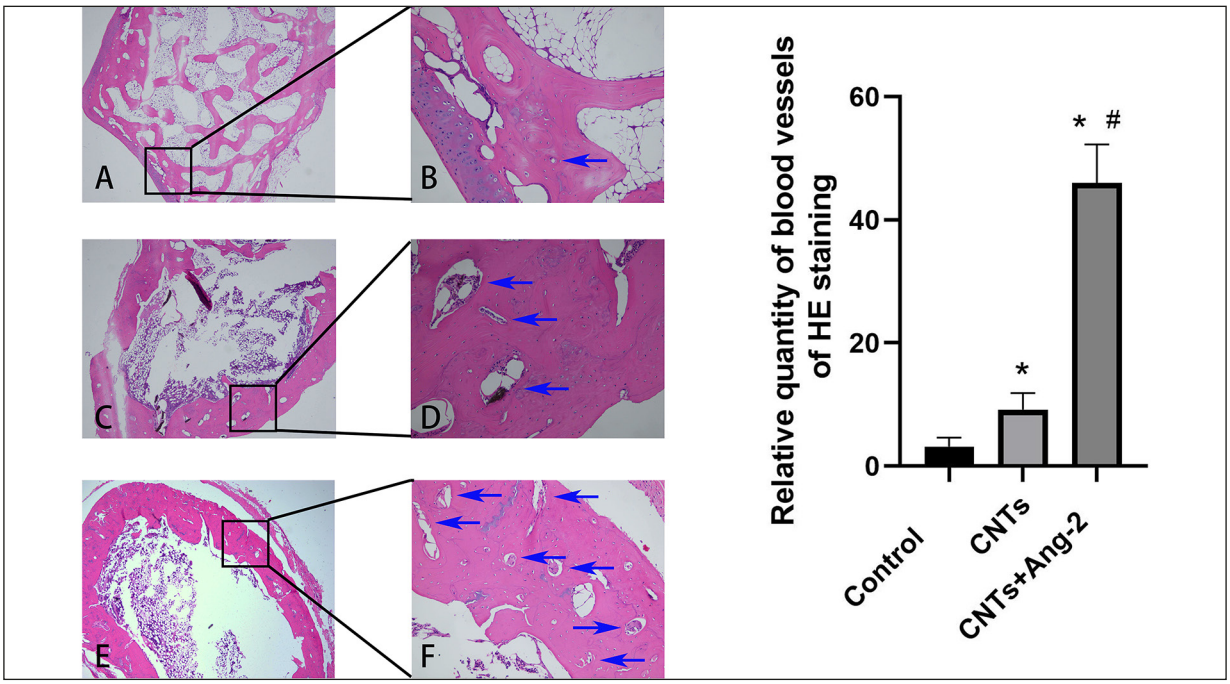

Figure 8. H and E staining of the bone defect area in each group at 12 weeks after surgery. Ang2 promoted angiogenesis and osteogenesis. **A-B**, Group A: Control group; **C-D**, Group B: CNTs/PLA/CHI group; **E-F**, Group C: CNTs/PLA/CHI + Ang-2 group. Magnification: left column ×40; right column ×200. Arrow: blood vessels. **F**, The values are expressed as the means ± SD (n = 6). *$p < 0.05$ *vs.* group control group; $^{\#}p < 0.05$ *vs.* CNTs group.

nied by dense trabecular bone and a predominant formation of lamellar bone (Figure 8E-F). There were many new blood vessels in the new bony callus. The number of blood vessels per slice in groups A, B, and C were (3.17 ± 1.47)/mm^2, (9.17 ± 2.71)/mm^2, and (46.00 ± 6.29)/mm^2, respectively. The number of blood vessels was significantly higher in group C than in groups A (t = -16.23, p = 0.000) and B (t = - 13.16, p = 0.000) and in group B than in group A (t = -4.76, p = 0.001), the difference was statistically significant respectively (Figure 8). Western blotting results suggested that the expressions of bone morphogenetic protein (BMP)-2 and VEGF in group C were significantly higher than those in groups A and B ($p < 0.05$) (Figure 9).

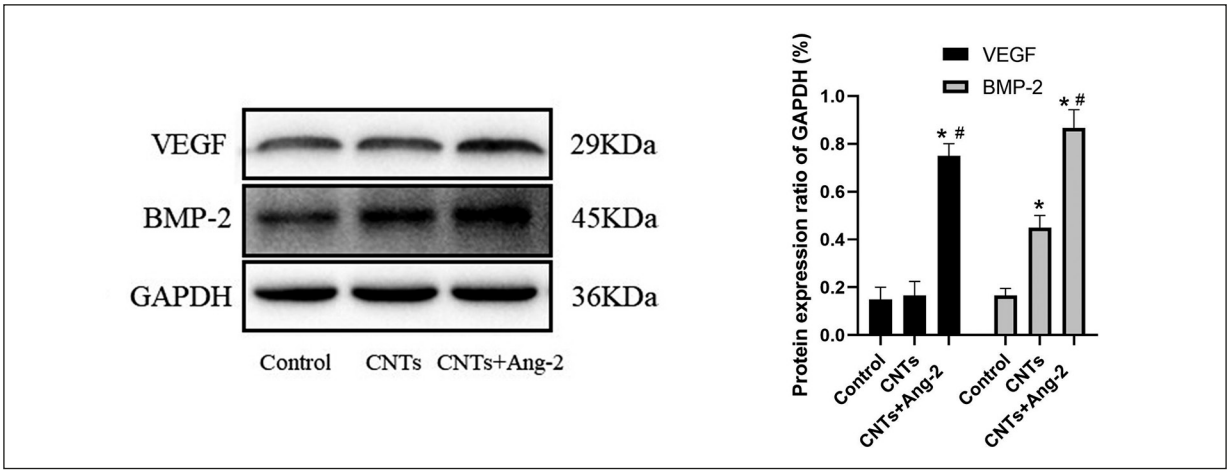

Figure 9. Ang-2 promoted the expression of VEGF and BMP-2 in the bone defect area. The expression levels of VEGF and BMP-2 were analyzed *via* western blot. Values are expressed as the means ± SD. The results represent relative expression levels. *$p < 0.05$ *vs.* control group; $^{\#}p < 0.05$ *vs.* CNTs group.

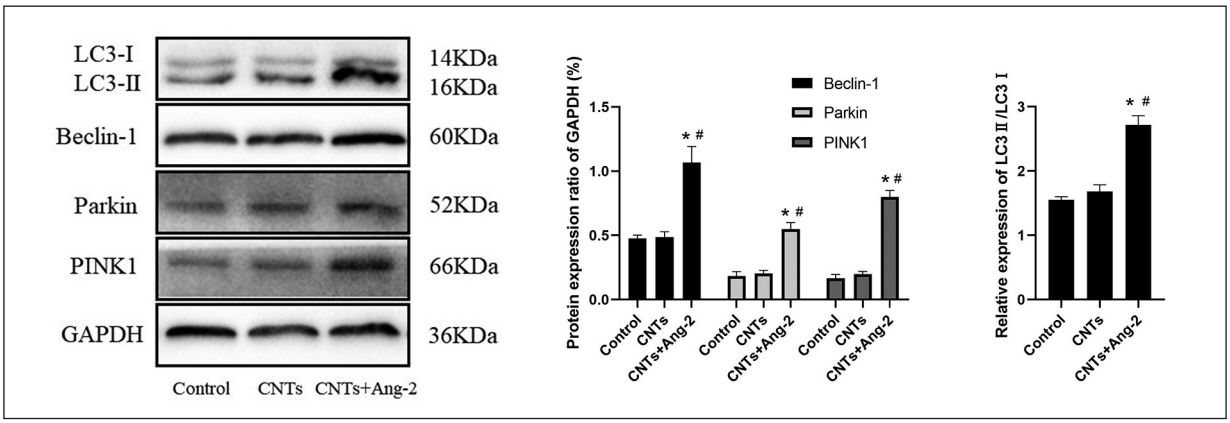

Figure 10. Ang-2 facilitated the expression of mitophagy proteins in the bone defect area. The expression levels of LC3 II/I, Beclin-1, Parkin and PINK1 were analyzed *via* western blot. Values are expressed as the means ± SD. The results represent relative expression levels. *$p < 0.05$ *vs.* control group; $^{\#}p < 0.05$ *vs.* CNTs group.

Ang-2 Promoted Mitophagy and Inhibits the Expression of Pyroptosis

Western blotting results indicated that the mitophagy-related protein expressions, such as LC3-II/I ratio, Beclin-1, Parkin and PINK1, in group C were significantly higher than those in groups A and B (Figure 10). Meanwhile, the pyroptosis-related protein expressions of NLRP3, GSDMD-N, caspase-1 p20 and IL-1β in group C were significantly lower than those of group A and group B (Figure 11). The molecular mechanism of this experiment is shown in Figure 12.

Discussion

The repair of CSD is still a difficult problem for orthopedic surgeons. Bone TE has the advantages of convenient and wide range of materials, biocompatibility, mechanical properties, good osteoinductive and osteogenic abilities, etc., which provides a new idea for the repair of bone defects[19]. At present, bone tissue biomaterials mainly include natural polymer materials, synthetic polymer materials, and bioceramic materials[20]. However, these three materials have different shortcomings in bone repair applications. Natural polymer materials, such as chitosan, collagen, etc., have uncontrolled biodegradation rates and poor mechanical stability, mechanical properties, and electrical properties, which are not suitable for simulating natural bone tissue matrix[21,22]. The hydrophilicity, cytocompatibility and mechanical properties of synthetic polymer materials are not satisfactory. Although bioceramics have been used in plastic surgery, oral and maxillofacial

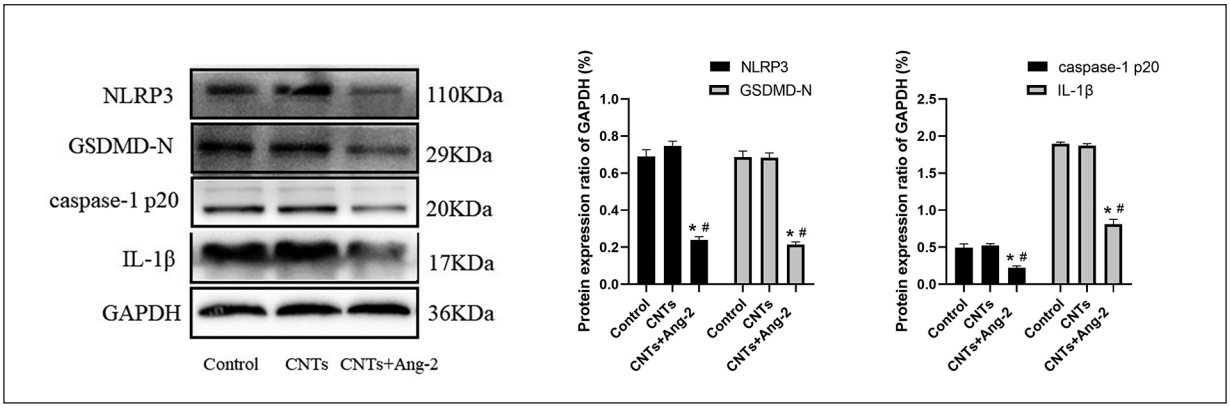

Figure 11. Ang-2 inhibited the expression of pyroptotic proteins in the bone defect area. The expression levels of NLRP3, GSDMD-N, caspase-1 p20 and IL-1β were analyzed *via* western blot. Values are expressed as the means ± SD. The results represent relative expression levels. *$p < 0.05$ *vs.* control group; $^{\#}p < 0.05$ *vs.* CNTs group.

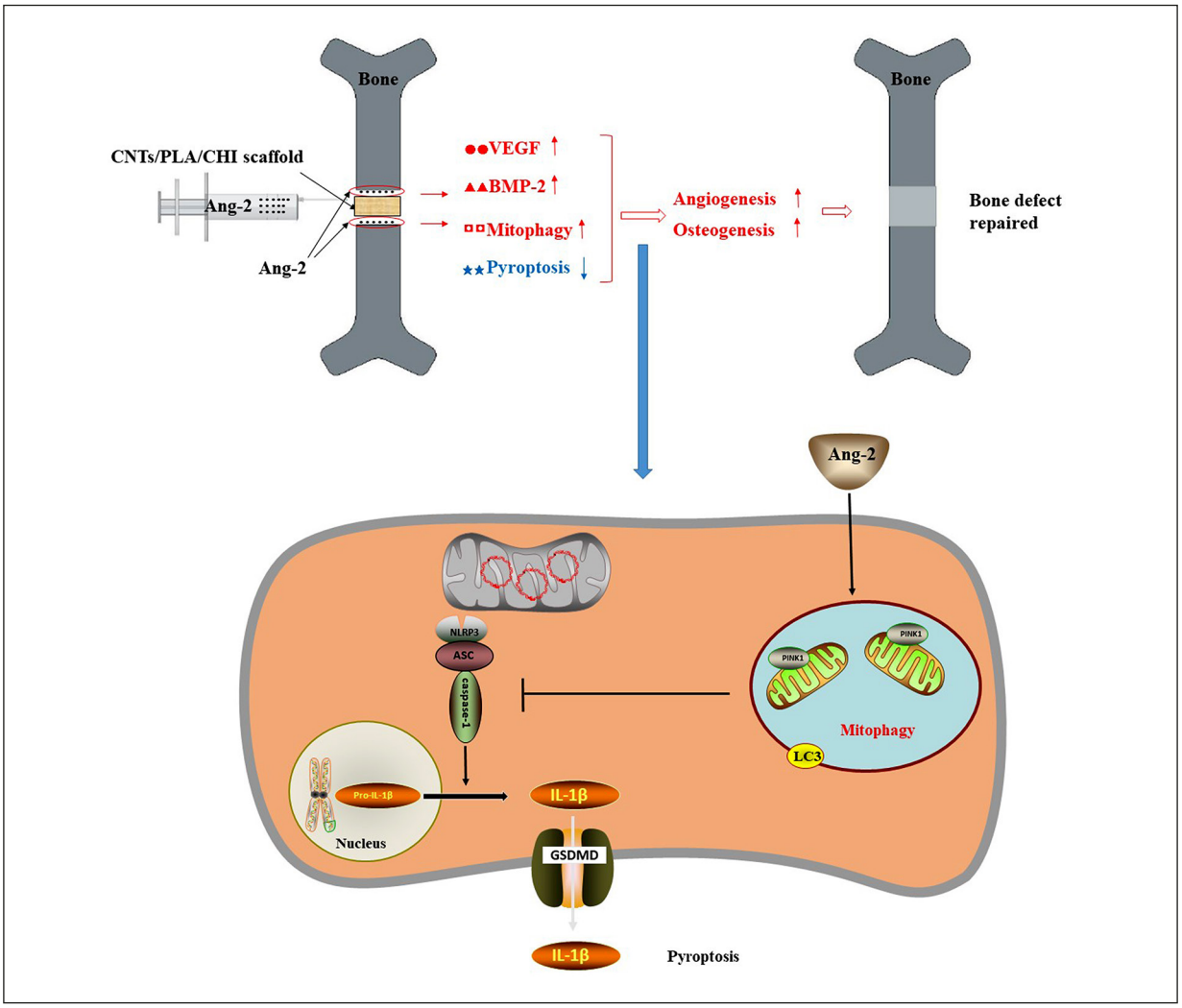

Figure 12. Mechanism of Ang-2 combined with CNTs/PLA/CHI three-dimensional porous scaffold to promote angiogenesis and bone defect repair by promoting mitophagy and inhibiting pyroptosis.

surgery or bone defect repair, their poor plasticity, high brittleness, and low flexural strength make them unsuitable as repair materials for CSD. Therefore, ideal bone TE materials should have good mechanical properties, biocompatibility, and controllable degradation rate. Despite all the definitions and expectations of a suitable scaffold, no material has yet been identified as an ideal scaffold in bone TE. Micro-nanoscale interconnected porous scaffolds with the properties of promoting blood vessel formation, cell adhesion and migration have become the expectation of many researchers.

CNTs have high mechanical strength and thermal stability. Studies[23] have confirmed that CNTs not only have good cytocompatibility, but also have the potential to promote cellular osteogenesis. In this research, the number of callus and the expression of BMP-2 in the CNTs/PLA/CHI group were significantly higher than those in the control group, although less than those in the CNTs/PLA/CHI + Ang-2 group, indicating that the CNTs/PLA/CHI scaffold has satisfactory osteogenesis. Optimizing the biological properties of carbon nanotubes is critical for their clinical and biological applications. Therefore, we prepared CNTs/PLA/CHI three-dimensional porous scaffolds with more comprehensive biological properties[24,25]. Surface modification of scaffold can greatly affect cell function, adhesion, growth, and other behaviors, as well as the biological properties of biomaterials[26,27].

The surface modification methods of materials generally include chemical modification, hybrid modification, plasma, and surface immobilization. By modifying the surface of the biological material to introduce substances with cell recognition signals, it is more suitable to adhere, extend and proliferate on the modified scaffold material. Due to the particularity of the preparation process of carbon nanotubes, some metal catalysts may remain, and these catalysts may adversely affect the growth of cells, so it is necessary to remove impurities before forming into scaffold materials. In order to remove impurities from CNTs, concentrated acid treatment was used in this experiment. Since CNTs are easy to agglomerate and are not easy to mix with other components such as polylactic acid and chitin, we used mixed strong acid to oxidize carbon nanotubes, that was, carboxylation.

SEM analysis revealed that the CNTs/PLA/CHI three-dimensional porous scaffolds have higher specific surface area, which is favorable for more protein adsorption and cell adhesion growth. It is especially important that the interconnected nanonetwork structure of the CNTs/PLA/CHI scaffold has appropriate porosity, which is conducive to the material exchange of scaffold with the extracellular matrix, thereby regulating cell morphology and promoting osteoblast differentiation.

The CNTs/PLA/CHI three-dimensional porous scaffolds we developed have suitable hydrophilic properties. The addition of CNTs will weaken the hydrophilicity of PLA/CHI materials, and materials with too strong hydrophilicity are not conducive to the adsorption of proteins and thus the adhesion of cells[28]. For highly hydrophobic surfaces, the adsorption of non-adhesive proteins on the material surface hinders the adsorption of adhesive proteins. In addition, the natural conformation of the molecular chain of the adhesion protein adsorbed on the surface of the highly hydrophobic material is destroyed, so that the active site in the protein molecular chain that binded to the integrin on the cell membrane surface cannot be fully exposed, which is not conducive to cell adhesion. On the surface with moderate hydrophilicity, the adhesion protein can not only adsorb on the surface of the material, but also maintain the natural conformation of the molecular chain, which is conducive to the normal adhesion of cells[29].

From the pH results, CHI hindered the decrease of the pH value of the material soaking solution. This is mainly due to the neutralization of the acidic degradation products of polylactic acid by the alkaline degradation products of chitin. Secondly, because the interface accelerates the diffusion of degradation products, local pH reduction was less likely to occur. Therefore, the "autocatalytic effect" of hydrolysis could be weakened and the matrix hydrolysis process could be slowed down. In addition, the fiber acted as a barrier to the diffusion of water molecules to ease the matrix hydrolysis process. The addition of CNTs did not affect the degradation rate of other components of the material. As the degradation progresses, a large number of micropores appeared on the surface and inside of the scaffold material, which helped the material to adsorb active proteins. The addition of CNTs was beneficial to slow down the reduction of the compressive strength of the material during the degradation process, thereby helping the material to play a better structural support role for the ingrowth of new bone tissue *in vivo*.

In previous studies, we have successfully prepared nano-hydroxyapatite/collagen/sodium alginate (nHAC/ALG) composite biomaterial, and verified its good physical properties in cell experiments, which can promote bone marrow mesenchymal stem cells differentiating into osteoblasts to repair bone defects[30]. One of the keys to the rapid survival of bone TE after implantation *in vivo* is vascularization. In the microenvironment of angiogenesis, a variety of cytokines and signaling pathways are involved in the formation of new blood vessels. Among them, the angiopoietin-tyrosine kinase receptors2 (Ang-Tie2) signaling axis plays an important role in the formation of new blood vessels. Ang-1 acts to stabilize blood vessels by affecting the junctions between endothelial cells (ECs) and the actin cytoskeleton. While Ang-2 is involved in the early initiation and excitation stages of angiogenesis[31]. In the initial stages of angiogenesis, separation between ECs and Sertoli cells is necessary. Ang-2 can competitively block the vascular stabilizing effect of Ang-1, making ECs into an unstable state and increasing the sensitivity to growth factors, thereby accelerating the formation of new blood vessels. Therefore, Ang-2 combined with TE scaffolds provide a new method to repair CSD. Our previous studies have found that local injection of Ang-2 can regulate autophagy and promote early vascularization and bone defect repair of hydroxyapatite/collagen scaffolds *in vivo*[17]. Since the tensile strength and toughness

of hydroxyapatite are not ideal, in order to further improve the material, we choose CNTs with lower price and better performance to improve the scaffold performance. The experimental results showed that the CNTs/PLA/CHI scaffold had a certain ability to repair bone defects but could not repair bone defects independently. When Ang-2 was applied locally, the number of new blood vessels in the bony callus increased significantly, accompanied by a stronger effect on bone defect repair.

In addition, we also found that the inflammatory tissue around the new callus area was significantly reduced after the application of Ang-2. To further explore the mechanism of Ang-2, western blotting results demonstrated that mitophagy in the callus area was significantly enhanced, while pyroptosis was significantly inhibited. Autophagy is an evolutionarily conserved catabolic process that degrades damaged proteins and organelles through lysosomes. Mitophagy, the selective autophagic degradation of damaged mitochondria, reduces the release of mitochondria-related inflammatory factors[32,33]. Pyroptosis is a novel pro-inflammatory mode of regulated cell death that plays a role in cellular inflammatory death in a variety of diseases[34]. NLRP3 is the most studied and understood of the inflammasomes to date[35]. In this study, the addition of Ang-2 reduced the activation of NLRP3 and caspase-1, the expression of the pyroptosis-dependent protein GSDMD, as well as the activation of the inflammatory factor IL-1β, which further demonstrated that Ang-2 promotes angiogenesis and repair of bone defects in tissue-engineered bone through the mitophagy-pyroptosis pathway. Therefore, we speculate that Ang-2 may inhibit pyroptosis by promoting mitophagy and attenuate cellular inflammatory death, thereby promoting neovascularization and repair of bone defects. Since the inhibitors of mitophagy and pyroptosis were not used as a control in the experiment, which is what our future work needs to do. The regulatory mechanism between mitophagy and pyroptosis, such as through ROS or double-stranded DNA, remains to be further elucidated.

Limitations

Despite the satisfactory results of animal experiments, there are still many challenges for clinical application of this method. Cytotoxicity and bioavailability of biomaterials will require comprehensive toxicological analysis. The controlled release effect of carbon nanotubes on drugs still needs to be developed. Additionally, Ang-2 is only used in the early stage of angiogenesis, and whether Ang-1 and/or VEGF has a further promoting effect in the later stage remains to be studied. In conclusion, CNTs/PLA/CHI scaffold combined with Ang-2 has potential application for bone regeneration, which brings hope to CSD patients.

Conclusions

CNTs/PLA/CHI scaffold has excellent biological properties. It combines with Ang-2 to accelerate the repair of critical-size bone defects by promoting mitophagy and inhibiting pyroptosis.

Conflict of Interest

The Authors declare that they have no conflict of interests.

Acknowledgements

Special thanks to Professor Xiaoming Li from key laboratory for biomechanics and mechanobiology of ministry of education, school of biological science and medical engineering (Beihang University), for his guidance on the CNTs/PLA/CHI three-dimensional porous scaffolds.

Ethics Approval

Animal experiments were approved by the Animal Care Committee of Nanjing Medical University (NJMU, Nanjing, China).

Funding

This work was supported by the Natural Science Foundation of Jiangsu Province (SBK2019022658), Nanjing Health Science and Technology Development Special Fund Project (ZKX22061 and YKK22222) and the Projects of Youth Innovation and Scientific Research Fund of the Affiliated Jiangning Hospital with Nanjing Medical University (JNYYZXKY202115).

Availability of Data

The data that support the findings of this study are available on request from the corresponding author.

Authors' Contribution

Xinhui Liu planned the study. Ziyi Tai and Qin Hu collected the data. Jian Yin did the analysis. Jian Yin and Ziyi Tai wrote the draft paper. Jian Yin, Yu Liu, Bin Wang and Chao Zhu involved in animal experiments. All authors contributed to and approved the final version of the manuscript.

References

1) Zhang X, Yin X, Luo J, Zheng X, Wang H, Wang J, Xi Z, Liao X, Machuki J O, Guo K, Gao F. Novel Hierarchical Nitrogen-Doped Multiwalled Carbon Nanotubes/Cellulose/Nanohydroxyapatite Nanocomposite As an Osteoinductive Scaffold for Enhancing Bone Regeneration. ACS Biomater Sci Eng 2019; 5: 294-307.
2) Careri S, Vitiello R, Oliva M S, Ziranu A, Maccauro G, Perisano C. Masquelet technique and osteomyelitis: innovations and literature review. Eur Rev Med Pharmacol Sci 2019; 23: 210-216.
3) Mukherjee S, Nandi S K, Kundu B, Chanda A, Sen S, Das P K. Enhanced bone regeneration with carbon nanotube reinforced hydroxyapatite in animal model. J Mech Behav Biomed Mater 2016; 60: 243-255.
4) Li X, Feng Q, Liu X, Dong W, Cui F. Collagen-based implants reinforced by chitin fibres in a goat shank bone defect model. Biomaterials 2006; 27: 1917-1923.
5) Zhang M, Lin R, Wang X, Xue J, Deng C, Feng C, Zhuang H, Ma J, Qin C, Wan L, Chang J, Wu C. 3D printing of Haversian bone-mimicking scaffolds for multicellular delivery in bone regeneration. Sci Adv 2020; 6: eaaz6725.
6) Li K, Wang D, Zhao K, Song K, Liang J. Electrohydrodynamic jet 3D printing of PCL/PVP composite scaffold for cell culture. Talanta 2020; 211: 120750.
7) Li X, Wang L, Fan Y, Feng Q, Cui F Z, Watari F. Nanostructured scaffolds for bone tissue engineering. J Biomed Mater Res A 2013; 101: 2424-2435.
8) Li X, Wang Z, Zhao T, Yu B, Fan Y, Feng Q, Cui FZ, Watari F. A novel method to in vitro evaluate biocompatibility of nanoscaled scaffolds. J Biomed Mater Res A 2016; 104: 2117-2125.
9) Mata D, Amaral M, Fernandes A J, Colaço B, Gama A, Paiva M C, Gomes P S, Silva R F, Fernandes M H. Diels-Alder functionalized carbon nanotubes for bone tissue engineering: in vitro/in vivo biocompatibility and biodegradability. Nanoscale 2015; 7: 9238-9251.
10) Gengenbacher N, Singhal M, Mogler C, Hai L, Milde L, Pari AAA, Besemfelder E, Fricke C, Baumann D, Gehrs S, Utikal J, Felcht M, Hu J, Schlesner M, Offringa R, Chintharlapalli S R, Augustin H G. Timed Ang2-Targeted Therapy Identifies the Angiopoietin-Tie Pathway as Key Regulator of Fatal Lymphogenous Metastasis. Cancer Discov 2021; 11: 424-445.
11) Antoniotti C, Marmorino F, Boccaccino A, Martini S, Antista M, Rossini D, Zuco V, Prisciandaro M, Conca V, Zucchelli G, Borelli B, Cosentino P, Germani M M, Bosco M F, Carullo M, Vetere G, Moretto R, Giordano M, Masi G, Pietrantonio F, Zaffaroni N, Cremolini C. Early modulation of Angiopoietin-2 plasma levels predicts benefit from regorafenib in patients with metastatic colorectal cancer. Eur J Cancer 2022; 165: 116-124.
12) Ten Voorde AMW, Wierenga APA, Nell RJ, van der Velden PA, Luyten GPM, Verdijk RM, Jager MJ. In Uveal Melanoma, Angiopoietin-2 but Not Angiopoietin-1 Is Increased in High-Risk Tumors, Providing a Potential Druggable Target. Cancers (Basel) 2021; 13.
13) Zhang S, Xie Y, Yan F, Zhang Y, Yang Z, Chen Z, Zhao Y, Huang Z, Cai L, Deng Z. Negative pressure wound therapy improves bone regeneration by promoting osteogenic differentiation via the AMPK-ULK1-autophagy axis. Autophagy 2022; 18: 2229-2245.
14) Zhu M, Wang Y, Zhu L, Du S, Wang Z, Zhang Y, Guo Y, Tu Y, Song E. Crosstalk Between RPE Cells and Choroidal Endothelial Cells via the ANXA1/FPR2/SHP2/NLRP3 Inflammasome/Pyroptosis Axis Promotes Choroidal Neovascularization. Inflammation 2022; 45: 414-427.
15) Li Z, Wu M, Liu S, Liu X, Huan Y, Ye Q, Yang X, Guo H, Liu A, Huang X, Yang X, Ding F, Xu H, Zhou J, Liu P, Liu S, Jin Y, Xuan K. Apoptotic vesicles activate autophagy in recipient cells to induce angiogenesis and dental pulp regeneration. Mol Ther 2022.
16) Annamalai RT, Turner PA, Carson WF 4th, Levi B, Kunkel S, Stegemann JP. Harnessing macrophage-mediated degradation of gelatin microspheres for spatiotemporal control of BMP2 release. Biomaterials 2018; 161: 216-227.
17) Yin J, Gong G, Sun C, Yin Z, Zhu C, Wang B, Hu Q, Zhu Y, Liu X. Angiopoietin 2 promotes angiogenesis in tissue-engineered bone and improves repair of bone defects by inducing autophagy. Biomed Pharmacother 2018; 105: 932-939.
18) Lane JM, Sandhu HS. Current approaches to experimental bone grafting. Orthop Clin North Am 1987; 18: 213-225.
19) Shi S, Wang XH, Guo G, Fan M, Huang MJ, Qian ZY. Preparation and characterization of microporous poly (D,L-lactic acid) film for tissue engineering scaffold. Int J Nanomedicine 2010; 5: 1049-1055.
20) Shi S, Jiang W, Zhao T, Aifantis K E, Wang H, Lin L, Fan Y, Feng Q, Cui F Z, Li X. The application of nanomaterials in controlled drug delivery for bone regeneration. J Biomed Mater Res A 2015; 103: 3978-3992.
21) Li J, Wang Q, Gu Y, Zhu Y, Chen L, Chen Y. Production of Composite Scaffold Containing Silk Fibroin, Chitosan, and Gelatin for 3D Cell Culture and Bone Tissue Regeneration. Med Sci Monit 2017; 23: 5311-5320.
22) Krishnakumar GS, Gostynska N, Campodoni E, Dapporto M, Montesi M, Panseri S, Tampieri A, Kon E, Marcacci M, Sprio S, Sandri M. Ribose mediated crosslinking of collagen-hydroxyapatite hybrid scaffolds for bone tissue regeneration using biomimetic strategies. Mater Sci Eng C Mater Biol Appl 2017; 77: 594-605.
23) Pei B, Wang W, Dunne N, Li X. Applications of Carbon Nanotubes in Bone Tissue Regeneration

and Engineering: Superiority, Concerns, Current Advancements, and Prospects. Nanomaterials (Basel) 2019; 9.

24) Siqueira IA, Corat MA, Cavalcanti B, Ribeiro Neto WA, Martin AA, Bretas RE, Marciano FR, Lobo AO. In Vitro and in Vivo Studies of Novel Poly (D, L-lactic acid), Superhydrophilic Carbon Nanotubes, and Nanohydroxyapatite Scaffolds for Bone Regeneration. ACS Appl Mater Interfaces 2015; 7: 9385-9398.

25) Xie J, Peng C, Zhao Q, Wang X, Yuan H, Yang L, Li K, Lou X, Zhang Y. Osteogenic differentiation and bone regeneration of iPSC-MSCs supported by a biomimetic nanofibrous scaffold. Acta Biomater 2016; 29: 365-379.

26) Sandanaraj BS, Vutukuri DR, Simard JM, Klaikherd A, Hong R, Rotello VM, Thayumanavan S. Noncovalent modification of chymotrypsin surface using an amphiphilic polymer scaffold: implications in modulating protein function. J Am Chem Soc 2005; 127: 10693-10698.

27) Pompe T, Keller K, Mothes G, Nitschke M, Teese M, Zimmermann R, Werner C. Surface modification of poly(hydroxybutyrate) films to control cell-matrix adhesion. Biomaterials 2007; 28: 28-37.

28) Chen BZ, Zhang LQ, Xia YY, Zhang XP, Guo XD. A basal-bolus insulin regimen integrated microneedle patch for intraday postprandial glucose control. Sci Adv 2020; 6: eaba7260.

29) Kumbar SG, Nukavarapu S , James R, Nair LS, Laurencin C T. Electrospun poly (lactic acid-co-glycolic acid) scaffolds for skin tissue engineering. Biomaterials 2008; 29: 4100-4107.

30) Liu X, Zhu C, Li Y, Yan Y, Hou C, Wang H, Yang Y, Guan G, Feng Q. The Preparation and In Vitro Evaluations of a Nanoscaled Injectable Bone Repair Material. Journal of Nanomaterials 2015; 2015: 858493.

31) Hilbert T, Poth J, Frede S, Klaschik S, Hoeft A, Baumgarten G, Knuefermann P. Anti-atherogenic effects of statins: Impact on angiopoietin-2 release from endothelial cells. Biochem Pharmacol 2013; 86: 1452-1460.

32) Li Q, Gao S, Kang Z, Zhang M, Zhao X, Zhai Y, Huang J, Yang G Y, Sun W, Wang J. Rapamycin Enhances Mitophagy and Attenuates Apoptosis After Spinal Ischemia-Reperfusion Injury. Front Neurosci 2018; 12: 865.

33) Chu C T. Mechanisms of selective autophagy and mitophagy: Implications for neurodegenerative diseases. Neurobiol Dis 2019; 122: 23-34.

34) Yu P, Zhang X, Liu N, Tang L, Peng C, Chen X. Pyroptosis: mechanisms and diseases. Signal Transduct Target Ther 2021; 6: 128.

35) Gangopadhyay A, Devi S, Tenguria S, Carriere J, Nguyen H, Jäger E, Khatri H, Chu L H, Ratsimandresey R A, Dorfleutner A, Stehlik C. NLRP3 licenses NLRP11 for inflammasome activation in human macrophages. Nat Immunol 2022; 23: 892-903.